Computational fluid dynamics for the influence of a semi-circular guiding wall on the hydraulic characteristics in an oxidation ditch

Wenli Wei*, Ch. Lou, Y. He, J. Wei, Y. Cai, Y. Chang

State Key Laboratory of Eco-hydraulics in Northwest Arid Region of China, Xi'an University of Technology, Xi'an, Shaanxi 710048, China, Tel. +86 15596886263; email: wei_wenli@126.com (W. Wei), Tel. +86 18292878016; email: 1398469272@qq.com (Ch. Lou), Tel. +86 18228318592; email: YHe2018@yean.net (Y. He), Tel. +86 18629352022; email: Jwei1995@126.com (J. Wei), Tel. +86 15191913820; email: Yxicai@126.com (Y. Cai), Tel. +86 13991987708; email: 564391746@qq.com (Y. Chang)

ABSTRACT

The flow field and velocity distribution were investigated by computational fluid dynamics (CFD) in a oxidation ditch (OD) with an semi-circular guiding wall to improve the flow mixture character and reduce energy consumption. The time-averaged gas–liquid two phase flow equations closed by the renormalized group (RNG) κ–ε model were solved by the semi-implicit method for pressure-linked equations (SIMPLE) algorithm, and the volume of fluid (VOF) method was applied to track the flow surface. The simulation results show that: (1) adding a semi-circular guiding wall can obviously reduce the size of circulation zone so as to make the effective volume of the OD become greater, and can result in the flow field distribution become more uniform so as to prevent sludge from settling, (2) the additional semi-circular guiding wall can make the percentage, P, of the VOF with a velocity greater than 0.3 m/s in the ditch be increased from 40.8% to 47.6% compared to that of the non-guiding wall, which is conducive to reducing sludge deposition in the OD, and (3) the additional semi-circular guiding wall can make the velocity value of outer high-speed flow decrease at the exit of the bend while the velocity value of inner low-speed flow increase, which makes the difference of velocity values between the inner and outer of the exit of the bend become small so as to obtain more uniform flow, and can effectively prevent sludge deposition in the bend of OD. The numerical simulation is an effective method to study the hydraulic characteristics of ODs, and simulation results have a certain guiding significance for reducing sludge deposition and improving the sewage treatment efficiency of ODs.

Keywords: Oxidation ditch; Numerical simulation; Semi-circular guiding wall; Submerged impellers

1. Introduction

Oxidation ditch (OD) is one of the improved activated sludge processes; it is a closed annular ditch, and is also called an annular aeration tank. Owing to the advantages of good effluent quality and simple system structure, OD plays an important role in urban sewage and industrial wastewater treatment systems [1]. The sewage treatment plants using OD process account for about 40% of the total number of small- and medium-sized sewage treatment plants in China; therefore, OD process has now become one of the main technologies of sewage treatment. At present, a lot of achievements have been obtained in all aspects of ODs, which mainly focus on: process design and equipment improvement, hydraulic characteristics test and flow simulation, bio-reaction kinetics, sludge migration, and sedimentation rate, simulation of gas distribution in ditches, etc.

The characteristics of flow fields are an important basis for the design and operation optimizations of a bioreactor

* Corresponding author.

[2]. For ODs, the shape of ditch, locations, and operation conditions of aeration and driving-flow equipment, and the setting guiding wall may significantly affect the hydraulic characteristics [3,4]. In recent years, with the rapid development of computational fluid dynamics (CFD), many scholars have made use of CFD to study the effect of guiding wall on the flow fields in ODs. Zhao et al. [5] numerically simulated the flow fields behind the diversion wall in an OD, pointing out that the diversion wall can improve the hydraulic conditions of the bend and the influence of the low-velocity zone (LVZ) behind the partition wall on mass transfer. Alaya et al. [6] simulated and measured oxygen concentrations for a wastewater treatment plant (WWTP), and obtained a good agreement for the oxygen concentration profiles. The validated model was used for simulating the oxygen concentration profiles in the ditch under different load conditions. Wei and Xu [7] simulated the influence of radius size of impellers on the cross-sectional average velocity of flow in an OD by solving the three-dimensional (3D) time-averaged Navier–Stokes equations with RNG k–ε turbulence model. According to the simulation results, the equation for the cross-sectional average velocity of flow varying with the radius size of impellers was obtained, which can provide an important reference in the optimization of designing impellers of the OD. Wei et al. [8] proposed a numerical simulation method for the flow fields, and used it to simulate longitudinal velocities along the representative vertical lines under working conditions of an Orbal OD. The comparison between the simulated longitudinal velocities and the experimental ones shows a better agreement, which essentially validates the reliability of the mathematical model for an Orbal OD. Huang et al. [9] presented a CFD model for predicting the flow field in an OD driven by a surface aerator. The improved momentum source term approach to simulate the flow field of the OD driven by an inverse umbrella surface aerator was developed and validated through experiments, and was found to have a lower computational expense, and to be simpler to process, and easier to use. Thakre et al. [10] studied the aeration efficiency and oxygen transfer coefficient and the influence of aeration system on the flow field structure of an OD driven by curved blades, by which the optimal combination of three blade parameters of the blade angle, immersion depth, and impeller speed, was obtained. The operating condition of an OD has a significant impact on energy consumption and the effluent quality of WWTPs. Yang et al. [11] proposed a CFD model to optimize the operating condition by considering two important factors: flow field and dissolved oxygen (DO) concentration profiles. The model is capable of predicting flow pattern and oxygen mass transfer characteristics in ODs equipped with surface aerators and submerged impellers, and the surface aerators and submerged impellers were simulated by a moving wall model and a fan model, respectively. Xie et al. [12] applied a two-phase (liquid–solid) CFD model to simulate the flow field and sludge settling in a full-scale Carrousel OD, by which an optimized operation scheme of the OD was proposed. Liu et al. [13] studied the operational conditions of simultaneous nitrification and denitrification (SND) in the channel of OD without the need for a special anoxic tank based on lab-scale and pilot-scale experiments using real domestic wastewater. The influence of sludge loading and component proportion in influent, temperature, hydraulic retention time (HRT), DO, and operational mode on SND was investigated.

Based on the above researches, we proposed a numerical simulation method to study the flow field and velocity distribution in a ditch with a semi-circular guiding wall when the underwater impeller and water surface aerator are running simultaneously in an OD. The effect of the installation of a semi-circular guiding wall on the flow field in the OD was mainly studied, which can provide a reference for the optimization design of ODs.

2. Mathematical model

2.1. Governing equations

The unsteady compressible flows are governed by the unsteady time-averaged mass and momentum conservation equations, and can respectively be written as follows [14–16]:

$$\frac{\partial \rho}{\partial t} + \frac{\partial (\rho u_i)}{\partial x_i} = 0 \tag{1}$$

and

$$\frac{\partial (\rho u_i)}{\partial t} + \frac{\partial (\rho u_i u_j)}{\partial x_j} = -\frac{\partial p}{\partial x_i} + \frac{\partial}{\partial x_j}\left[\mu\left(\frac{\partial u_i}{\partial x_j} + \frac{\partial u_j}{\partial x_i}\right)\right] - \frac{\partial}{\partial x_j}\left(\rho \overline{u_i' u_j'}\right) + \rho g_i \tag{2}$$

where ρ is density; t is time; x_i is the space coordinate in i direction; p is pressure; μ is molecular kinematic viscosity; μ_t is kinematic viscosity; g_i is the gravitational acceleration in i-direction; u_i and u_i' are the time-averaged and fluctuating velocity components in i-direction, respectively; and the subscripts $i, j = 1, 2, 3$.

The Reynolds-averaged N–S equations are always closed by the turbulence models, such as the standard k–ε model, and the relatively improved models named as the RNG k–ε model and realizable k–ε model in CFD [17–19]. Here, the RNG k–ε model is used to close the Reynolds-averaged N–S equations, because it is suitable for describing the flows with curved streamlines in ODs.

The term, $\rho \overline{u_i' u_j'}$, in Eq. (2), is defined as Reynolds stress often modeled by the Boussinesq hypothesis relating these stresses to the mean deformation rates and mean velocity gradients [20], and can be written as:

$$-\rho \overline{u_i' u_j'} = \mu_t\left(\frac{\partial u_i}{\partial x_j} + \frac{\partial u_j}{\partial x_i}\right) - \frac{2}{3}\left(\rho k + \mu_t \frac{\partial u_i}{\partial x_i}\right)\delta_{ij} \tag{3}$$

where μ_t is the turbulent viscosity computed as a function of turbulent kinetic energy k and kinetic energy dissipation rate ε, and can be written as:

$$\mu_t = \rho C_\mu \frac{k^2}{\varepsilon} \tag{4}$$

with C_μ being a model constant of 0.085.

In the RNG k–ε turbulence model, the transport equations for k and ε are given by [14,17–19]:

$$\frac{\partial(\rho k)}{\partial t} + \frac{\partial(\rho k u_i)}{\partial x_i} = \frac{\partial}{\partial x_j}\left[\left(\mu + \frac{\mu_t}{\sigma_k}\right)\frac{\partial k}{\partial x_j}\right] + G_k - \rho\varepsilon \tag{5}$$

and

$$\frac{\partial(\rho\varepsilon)}{\partial t} + \frac{\partial(\rho\varepsilon u_i)}{\partial x_i} = \frac{\partial}{\partial x_j}\left[\left(\mu + \frac{\mu_t}{\sigma_\varepsilon}\right)\frac{\partial\varepsilon}{\partial x_j}\right] + C_1\frac{\varepsilon}{k}G_k - \rho C_2\frac{\varepsilon^2}{k} \tag{6}$$

where σ_k, C_2, and σ_ε are empirical constants with a value of 0.7179, 1.68, and 0.7179, respectively; and the other parameters are:

$$C_1 = 1.42 - \tilde{\eta}\left(1 - \tilde{\eta}/\tilde{\eta}_0\right)/\left(1 + \beta\tilde{\eta}^3\right), \tilde{\eta} = sk/\varepsilon, S = \left(2S_{i,j}S_{i,j}\right)^{1/2},$$

$$\tilde{\eta}_0 = 4.38, \beta = 0.015, \text{ and } S_{i,j} = \left(\frac{\partial u_i}{\partial u_j} + \frac{\partial u_j}{\partial u_i}\right).$$

2.2. Volume of fluid method

The volume of fluid (VOF) method [21] is used to track the liquid/gas interface. The volume fraction of liquid, F, in a cell, is defined as the ratio of the volume occupied by liquid to the total volume of the control cell. The value of F ranges between 0 and 1. $F = 1$ and 0 represent a control cell completely filled with liquid and gas, respectively; and $0 < F < 1$ represents a control cell partly filled with liquid, which shows the interface of liquid and gas. The value of F can be obtained by solving a separate passive transport equation, given by:

$$\frac{\partial F}{\partial t} + \frac{\partial(Fu_i)}{\partial x_i} = 0 \tag{7}$$

The physical properties, ρ and μ, of the mixture of gas and water appearing in the transport Eqs. (1)–(3), (5), and (6), are determined by the presence of water and air in each control volume, and can be computed by the following equations [21]:

$$\rho = \left(1 - F\right)\rho_a + F\rho_w \tag{8}$$

$$\mu = \left(1 - F\right)\mu_a + F\mu_w \tag{9}$$

where ρ_a and μ_a are the density and viscosity of air, respectively; ρ_w and μ_w are the density and viscosity of water, respectively.

3. Numerical simulations

3.1. Computational region

The simulation model is an OD with a height of 7.5 m. Its straight channel has a width of 9.5 m and a length of 26 m; the right-hand side semi-circular guiding wall has a radius of 4.75 m; and the middle baffle has a length of 26 m. The effective water depth is 4.24 m. The underwater impeller consists of eight blades, each of which is 1.132 m long and 0.5 m high; the distance from the center of the impeller to the left-hand end of the central baffle is 2.6 m; and the bottom

of the impeller is 1.0 m away from the water surface in the vertical direction. The impeller rotates counter-clockwise at 29.01 rpm (3.03 rad/s). The water surface aerator with a radius of 1.5 m consists of 19 discs, and the nearby discs have an interval of 0.5 m; it is installed at middle of the straight channel, and with a height of 4.74 m of its central axis, and it rotates at 2.5 rad/s. The details of the model size are shown in Fig. 1, and the computational region is shown in Figs. 2a and b:

3.2. Grid generation

The combination of structured and unstructured grids was used to obtain a high-quality computational grid generated by GAMBIT software. The calculation area of the OD was simulated under two working conditions of (a) with a semi-circular guiding wall and (b) without semi-circular guiding wall, such as in Figs. 2a and b. Compared with the whole calculation area, the thickness of the impeller and the blade of aerators are very small; in order to ensure the grid quality, the impeller and the blades of the aerator were simplified to be infinitely thin. The total number of mesh elements is 268,875. The grid generation method and the grid structure are basically the same under the two conditions. Figs. 3a and b show the 2D plane grid and 3D grid of the OD with a semi-circular guiding wall, respectively.

The independence of the computational grid has been validated to meet the requirement of the simulation. Using the same initial and boundary conditions, the flow fields for the OD with 235,866; 268,875; and 282,375 meshes are numerically computed, respectively, which shows that the computational grid with 268,875 meshes is an independent grid.

3.3. Initial and boundary conditions and solution method

The initial conditions are defined as an initial water depth of 4.24 m and an initial velocity, 0, of fluid in the OD. The relative motion of underwater impeller and water surface aerator for the OD was simulated by a multi-reference frame (MRF) system. The rotational speeds of aerator and impeller are 2.5 and 3.03 rad/s, respectively. The rotational reference system for both the impeller and aerator was established independently within the radii of the impeller and the aerator, and the relative velocities of the impeller and aerator are 0; in addition, the other fluid areas were set up as a stationary coordinate system. The semi-circular guiding wall, baffle, dich wall, and bottom wall are taken as solid-walls; the boundary conditions on solid wall are given
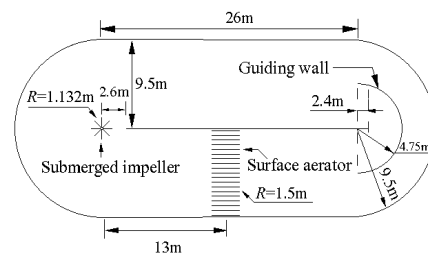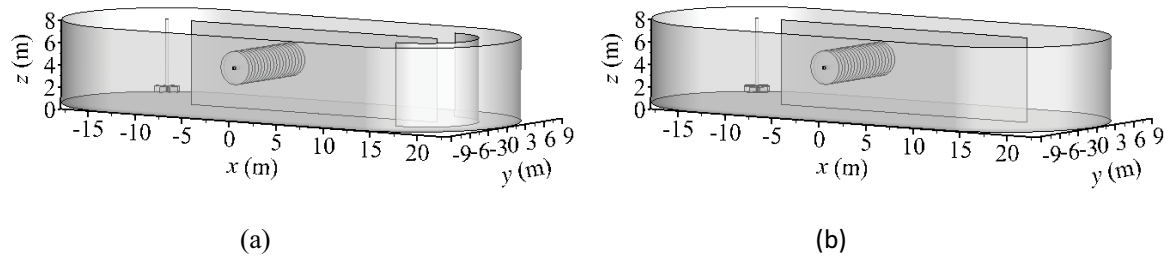

Fig. 1. Details of the model size.

Fig. 2. Computational region. (a) With and (b) without semi-circular guiding wall.
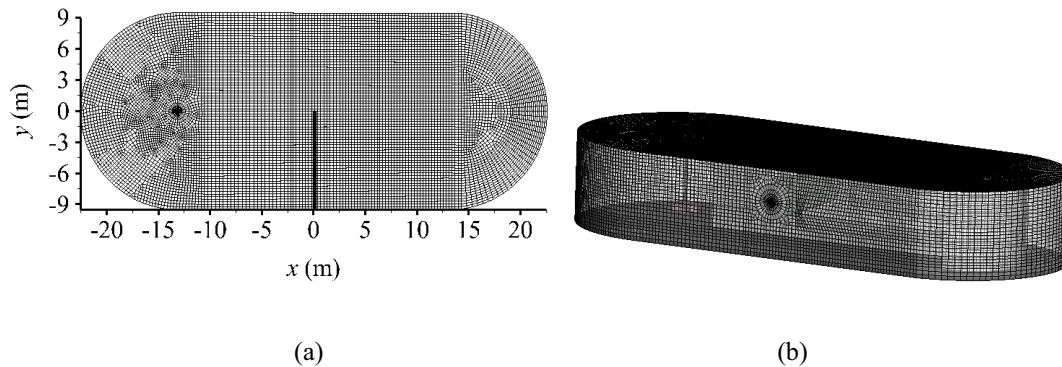

Fig. 3. Grids of the computational domain. (a) 2D plane grid and (b) 3D grid.

by a wall-function. The top surface of the computational domain is a pressure outlet with a relative pressure of 0. The free water surface was determined by the VOF method.

In the solution of the time-averaged N–S equations closed with RNG κ–ε turbulence model, the convection term was discretized by the first-order upwind method, and the pressure and velocity were coupled by SIMPLE algorithm. The time step is 0.005 s, and the calculation is convergent at 300 s.

4. Analyses of the results

4.1. Analysis of the streamlines of the flow field

Figs. 4a–d show the streamlines at a plane of $z = 3.775$ and 3.27 m (away from the bottom of ditch), respectively, when the underwater impeller and water surface aerator are running simultaneously with and without a semi-circular guiding wall.

It can be seen from Figs. 4a and c that when the semi-circular guiding wall is not added, there will form a large circulation zone near the exit of the bend, which is easy to cause sludge deposition in this area. The complex flow pattern and the non-uniform velocity distribution in the OD are mainly caused by the existence of bends. The concave wall of the right-hand side bend changes the direction of the flow, the inertia force acting on the flow impacts the concave wall, and the concave wall exerts a reaction force on the flow, forcing the flow to change its direction and run along the concave wall. The change of momentum of the flow results in the redistribution of the flow velocity at the exit of the right-hand side bend, which forms a larger recirculation zone downstream of the right-hand side bend.

As can be seen from Figs. 4b and d, after adding the semi-circular guiding wall, the flow in the right-hand side bend is divided into two parts: one is the flow between the semi-circular guiding wall and the concave wall, which does not produce a circulation; the other is the flow at the left-hand side of the semi-circular guiding wall, which does produce a circulation. The amount of circulation water is reduced, thus, the length and width of the circulation zone are obviously reduced compared to that of non-guiding wall, and the flow field distribution out of the circulation zone becomes more uniform. In addition, the larger the channel radius is, the smaller is the inertial force acting on a unit mass fluid, and vice versa. Adding the semi-circular guiding wall divides the entire channel into two narrow channels; the radius of the channel at the left-hand side of the semi-circular guiding wall is smaller than that between the semi-circular guiding wall and the concave wall, thus, the inertial force acting on a unit mass fluid is bigger at the left-hand side of the semi-circular guiding wall than that between the semi-circular guiding wall and the concave wall. But the semi-circular guiding wall prevent the flows exchange movement in the two separated bend channels, while with no guiding wall, the entire flow in the entire channel exchange movement; therefore, the circulation zone with no guiding wall is bigger than that of the semi-circular guiding wall.

4.2. Analysis of the contour profiles of velocity and turbulent kinetic energy at a plane

Figs. 5a and b show the simulated water surface positions in the OD with and without a semi-circular guiding wall at the right-hand side, respectively. Except for the fluctuation
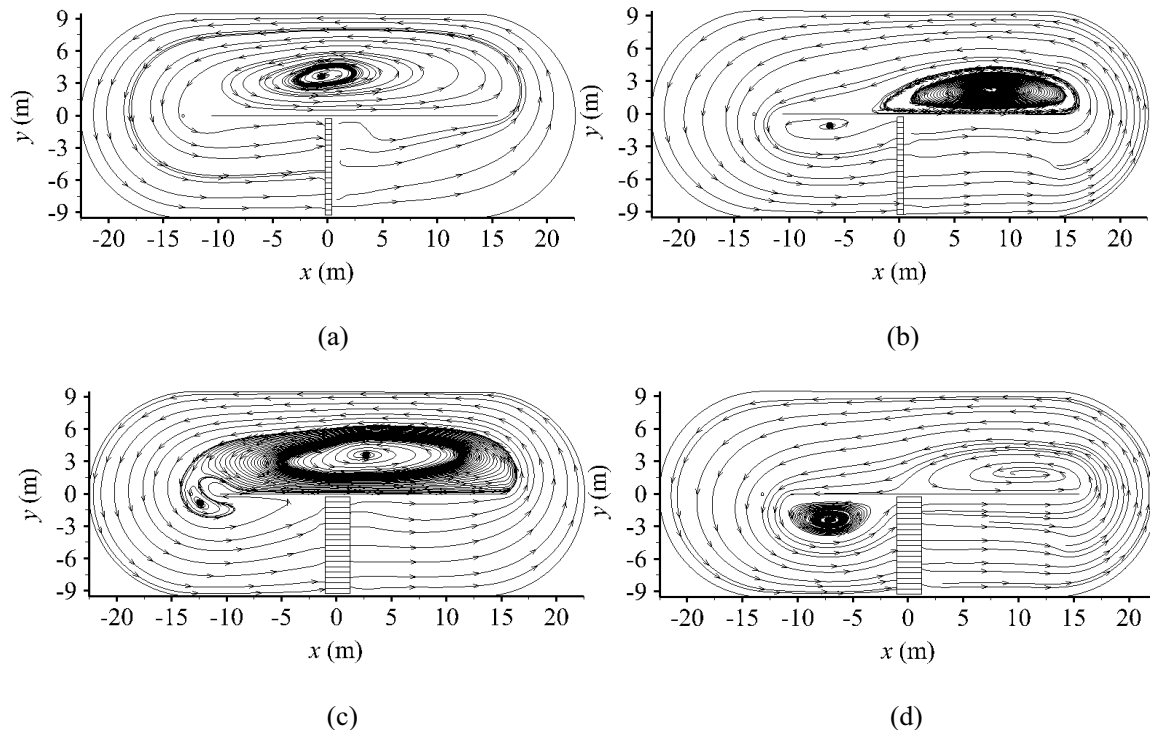
Fig. 4. Computed streamlines at a plane of $z = 3.27$ and 3.775 m. (a) Without guiding wall, $z = 3.27$ m, (b) with a semi-circular guiding wall, $z = 3.27$ m, (c) without guiding wall, $z = 3.775$ m, and (d) with a semi-circular guiding wall, $z = 3.775$ m.

near the surface aerator, the water surface is near a horizontal plane. There is some water on the surface aerator, which is caused by the viscosity of water and the inertia action of the rapid running aerator. Physical variables such as velocity and turbulent kinetic energy at a horizontal plane of $z = 3.775$ m (away from the bottom of ditch) are selected below the water surface for analysis.

Figs. 6a and b show the contours of velocity with colorful legend at a plane of $z = 3.775$ m (away from the bottom of ditch), when the underwater impeller and water surface aerator are running simultaneously with and without a semicircular wall, respectively. The comparison of Figs. 6a and b show that the velocity distribution in the OD with a wall is obviously more uniform than that of non-wall. With a wall, only a small area of lower velocity zone in the upper ditch appears near the central straight plate; while without a wall, there is a larger area of lower-velocity in the lower straight channel and at the right-hand side of the OD. The contours of flow velocity show that, with a wall, the maximum velocity is 0.9 m/s at the entrance of the outer bend near the wall, and the minimum is 0.1 m/s at the upper side of the central straight wall; while without a wall, the maximum velocity in the ditch is 0.05m/s in the central part of the upper ditch, and the minimum velocity is 0.009 m/s at the almost total right-hand side of the lower ditch.

Figs. 7a and b show the contour profiles of turbulent kinetic energy at a plane of $z = 3.775$ m (away from the bottom of ditch), when the underwater impeller and water surface aerator are running simultaneously with and without a guiding wall, respectively. By comparison of Figs. 7a and b, it can be found that the distribution of turbulent kinetic energy in the OD is affected by the addition of the semi-circular

wall. The turbulent kinetic energy at the right-hand side can reach 0.021 m²/s² with the semi-circular wall (in Fig. 7a), while in the same area only reaches 0.009 m²/s² without the wall (in Fig. 7b). The high-energy liquid flow mixes with that in the middle and lower parts of the OD, which makes energy distribution more uniform in the OD so as to prevent sludge deposition.

4.3. Analysis of the velocity distributions along the vertical lines

In order to more intuitively observe and analyze the velocity distributions along the vertical lines in the OD, the eight points of 1–5 and 2′–4′, as shown in Fig. 8, were selected as the positions of the vertical lines to extract the simulated velocity values to verify the improvement of flow velocity after adding a semi-circular guiding wall. Table 1 shows the coordinates of the eight points of 1–5 and 2′–4′.

In this study, with the rotating speeds of the underwater impeller and water surface aerator being constant, the velocity distributions along the eight vertical lines are extracted for the comparison of change of the flow velocities between the two working conditions: (a) with a semi-circular guiding wall and (b) without guiding wall, as shown in Fig. 9.

Fig. 9 shows that, after adding a semi-circular guiding wall, at the locations being nearer to the right-hand side concave wall, the flow velocities along the four vertical lines (at points 2–5) increases obviously, except that along the vertical line (at point 1) decrease slightly; at the locations away from the right-hand side concave wall, the flow velocities along the 2 vertical lines (at points 3′ and 4′) decrease obviously, except that along the vertical line (at point 2′)
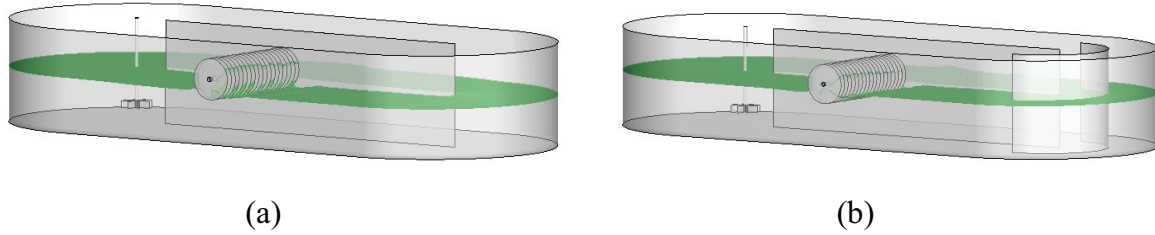
Fig. 5. Simulated water surface positions in the OD: (a) without a semi-circular guiding wall and (b) with a semi-circular guiding wall at the right-hand side.
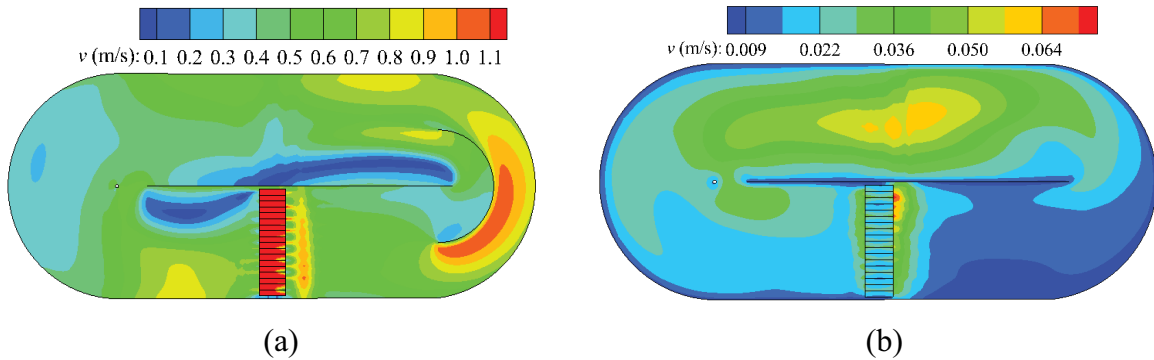

Fig. 6. Contour profiles of velocity at a plane of $z = 3.775$ m (away from the bottom of ditch). (a) With a semi-circular guiding wall and (b) without guiding wall.
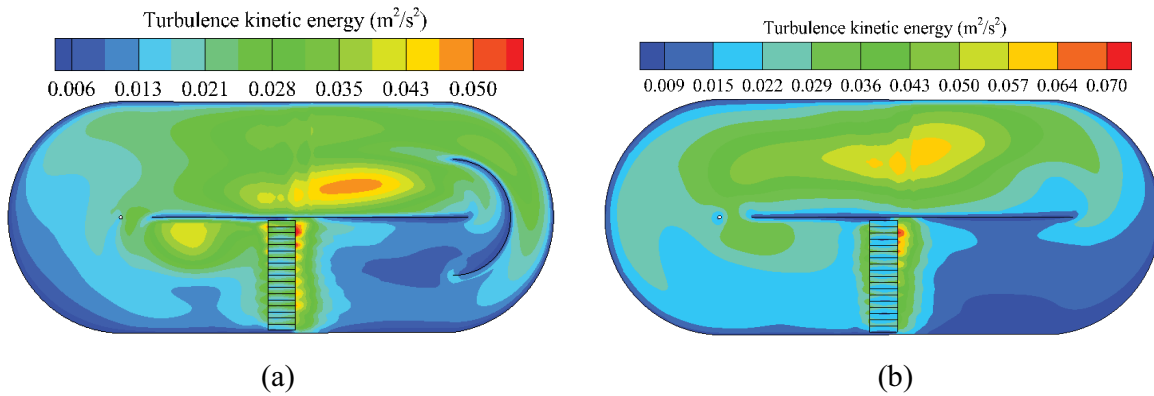

Fig. 7. Contour profiles of turbulent kinetic energy at a plane of $z = 3.775$ m (away from the bottom of ditch). (a) With a semi-circular guiding wall and (b) without guiding wall.

changes slightly. The cause for this phenomenon is that the setting of the bend semi-circular guiding wall separates the entire bend channel into two narrow bend channels, and the flow in the inner curved channel with greater inertial force per unit mass cannot exchange movement with that in the outer curved channel of smaller inertial force per unit mass by the baffling of the semi-circular guiding wall so as to weaken the role of the transverse circulation, and thus, the semi-circular guiding wall reduce the factors of generation of circulation, and also significantly improve the overall flow velocity in the bend of the OD.

Generally speaking, for a bend flow, the velocity near the outer concave wall is larger than that at the inner place over the exit cross-section of the bend [22]. From Figs. 9a
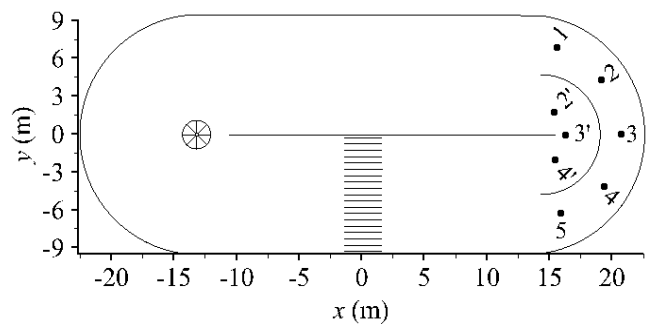

Fig. 8. Positions of the eight vertical lines.

Table 1
Coordinates of the eight points of 1–5 and 2′–4′

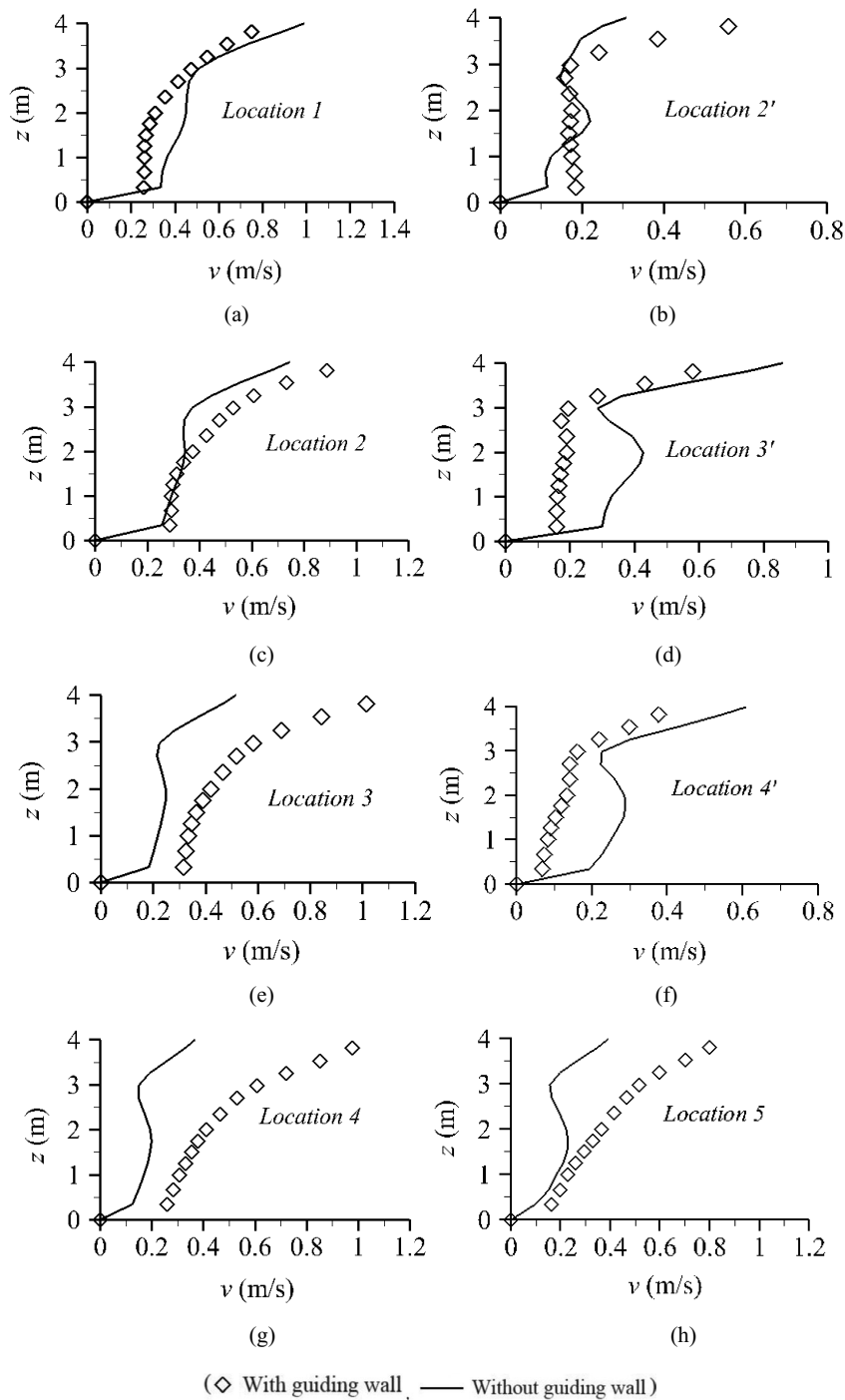| Points	1	2	2′	3	3′	4	4′	5
Coordinates (x)	14.2	18.9	15.9	20.7	16.6	18.9	15.9	14.2
Coordinates (y)	7.09	4.89	1.68	0	0	−4.98	−1.68	−7.09
Coordinates (z)	7.5	7.5	7.5	7.5	7.5	7.5	7.5	7.5

Fig. 9. Velocity distributions along the eight vertical lines. (a) Location 1, (b) location 2′, (c) location 2, (d) location 3′, (e) location 3, (f) location 4′, (g) location 4, and (h) location 5.

and b, it can be seen that, when the semi-circular guiding wall is added, the velocity value of outer high-speed flow decreases at the exit of the bend while that of the inner low-speed flow increases, which makes the difference of velocity values between the inner and outer of the exit of the right-hand side bend be small so as to obtain more uniform flow. This flow pattern can reduce the LVZ of the inner area of the right-hand side bend, and can effectively prevent sludge deposition in the right-hand side bend.

4.4. Statistical analysis of the velocity values in the OD

In order to prevent sludge from deposition in ODs, the design specifications for ODs require that the average velocity over a cross-section of an OD should be greater than 0.3 m/s [23]. Here, the percentage P of the VOF with velocity greater than 0.3 m/s to the VOF in the entire fluid region is taken as a parameter for the statistical analysis of the two cases: (a) with a semi-circular guiding wall and (b) without guiding wall, which are plotted in Fig. 10.

Fig. 10 shows that, under the simultaneous running of the underwater impeller and water surface aerator, the additional semi-circular guiding wall has a greater impact on the velocity distribution in the OD; and makes the percentage P in the ditch be increased from 40.8% to 47.6% compared to that of non-guiding wall. Therefore, the existence of a semi-circular guiding wall can not only reduce the size of circulation zone obviously, but also significantly improve the percentage P of the VOF with velocity greater than 0.3 m/s to the VOF in the entire fluid region, which is conducive to reducing sludge deposition in the OD.

5. Some discussions and further study plan

Numerical simulation and experimental methods are dependent upon each other; experiment is the main way to investigate a new basic phenomenon, taking a large amount of observation data as the foundation, still, the validation for a numerical simulation result must use the measured (in a prototype or a model) data. Doing numerical simulation in advance can obtain the preliminary results, which can make the corresponding experiment plan be more purposeful, and often reduces the number of systematical experiments; therefore, it is much useful for the design of experimental device [23].

Here, an experimentally validated numerical simulation method has been used to study the effect of the installed semi-circular guiding wall on the flow fields in an OD. Next, further study will be done to validate the simulation model by an experimental method. An experimental model for the Carrousel OD will be made of organic glass, according to the gravity similarity law (also named Froude number similarity theory) [24]. Acoustic Doppler velocimetry (ADV) will be used to measure velocities of the test model for the OD under the working condition with or without a semi-circular guiding wall to validate the reliability of the simulation results. Adding a guiding wall results in the flow field distribution become more uniform so that sludge can be prevented from settling in an OD, which will be verified by liquid–solid two phase simulation in the OD in the future.
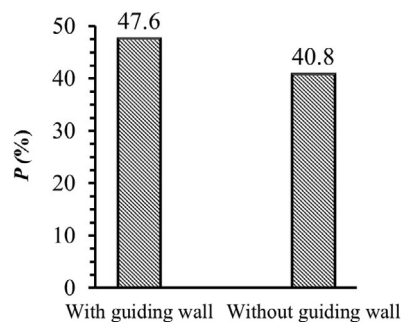

Fig. 10. Statistical analysis of velocity distribution.

6. Conclusions

A gas–liquid two-phase flow model was used to simulate the flow fields in an OD for two cases with and without a semi-circular guiding wall under the simultaneous running of underwater impeller and water surface aerator, by which the flow field structures and velocity distributions of different sections were obtained and analyzed. The conclusions are as follows:

- Adding a semi-circular guiding wall can obviously reduce the size of the circulation zone so as to make the effective volume of the OD become greater, and can result in the flow field distribution become more uniform so as to prevent sludge from settling.
- The additional curved semi-circular guiding wall can make the percentage, P, of the VOF with velocity greater than 0.3 m/s in the ditch be increased from 40.8% to 47.6% compared to that of no guiding-wall, which is conducive to reducing sludge deposition in the OD.
- The additional curved semi-circular guiding wall can make the velocity value of the outer high-speed flow decrease at the exit of the right-hand side bend while the velocity value of the inner low-speed flow increase, which makes the difference of velocity values between the inner and outer of the exit of the right-hand side bend become small so that more uniform flow can be obtained. This flow pattern can be useful for preventing sludge deposition in the bend of the OD.
- The numerical simulation is an effective method to study the hydraulic characteristics of ODs. The simulation results have a guiding significance for the setting of a semi-circular guiding wall to reduce sludge deposition and improve sewage treatment efficiency of the OD.

Symbols

C_μ — Model parameter in Eq. (4) with a value of 0.085
C_1' — Model parameter in Eq. (6)

C_2 — Model parameter in Eq. (6) with a value of 1.68
F — Volume fraction of liquid
g_i — Gravitational acceleration in i-direction, i = 1, 2, 3, m/s^2
k — Turbulent kinetic energy, m^2/s^2
p — Pressure, kg/m×s^2
G_k — Production term in Eqs. (5) and (6)
S — Parameter for computing C_1
$S_{i,j}$ — Parameter for computing C_1
t — Time, s
u_i — Velocity component in i-direction, i = 1, 2, 3, m/s
u_i' — Fluctuating velocity component in i-direction, i = 1, 2, 3, m/s
x_i — Space coordinate in i-direction, i = 1, 2, 3, m

Greek

β — A constant of 0.015 for computing C_1
δ_{ij} — Kronecker function in Eq. (3), δ_{ij} = 1 with $i = j$, and δ_{ij} = 0 with $i \neq j$
ε — Kinetic energy dissipation rate, m^2/s^3
$\tilde{\eta}$ — Parameter for computing C_1
$\tilde{\eta}_0$ — A constant of 4.38 for computing C_1
μ — Molecular kinematic viscosity, kg/ms
μ_t — Turbulent kinematic viscosity, kg/ms
ρ — Density, kg/m^3
σ_k — Model parameter in Eq. (5) with a value of 0.7197
σ_ε — Model parameter in Eq. (6) with a value of 0.7197

Subscripts

i,j — Direction i = 1, 2, and 3; j = 1, 2, and 3
t — Turbulence
a — Air
w — Water

References

[1] Z. Li, Y. Guo, M. Xing, P. Jin, X. Wang, M. Wu, The analysis of nitrification of upgrading on a carrousel oxidation ditch in Kunming, Tech. Water Treat., 40 (2014) 123–127.
[2] R. Deng, X. Zhang, J. Pan, R. Chen, Experimental research on circular the cyclic flow of mixing liquor in the integrated oxidation ditch, Water Wastewater Eng., 24 (1998) 12–17 (in Chinese).
[3] Y. Tang, Present situation and prospect of numerical simulation for flow field characteristics in oxidation ditch, J. Water Res. Archit. Eng., 10 (2012) 107–112 (in Chinese).
[4] T. Nameche, J.L. Vasel, Hydrodynamic studies and modelization for aerated lagoons and waste stabilization ponds, Water Res., 32 (1998) 3039–3045.
[5] X. Zhao, X. Wang, Y. Huang, Study on simulation of research settling sludge in curved conduit of oxidation ditch, Environ. Eng., 25 (2008) 37–39 (in Chinese).
[6] S.B. Alaya, L. Haouech, H. Cherif, H. Shayeb, Aeration management in an oxidation ditch, Desalination, 252 (2010) 172–178.
[7] J. Wei, Z. Xu, CFD method for the relationship between the radius size of impellers and cross-sectional average velocity of flow in an oxidation ditch, Desal. Water Treat., 126 (2018) 127–134.
[8] W. Wei, X. Chen, W.L. Lou, Y. Cai, J. Wei, Y. Zheng, CFD method for the liquid–gas two-phase flow fields in an Orbal oxidation ditch, Desal. Water Treat., 126 (2018) 135–143.
[9] W. Huang, K. Li, G. Wang, Y. Wang, Computational fluid dynamics simulation of flows in an oxidation ditch driven by a new surface aerator, Environ. Eng. Sci., 30 (2013) 663–671.
[10] S.B. Thakre, L.B. Bhuyar, S.J. Deshmukh, Oxidation ditch process using curved blade rotor as aerator, Int. J. Environ. Sci. Technol., 6 (2009) 113–122.
[11] Y. Yang, J. Yang, J. Zuo, Y. Li, S. He, X. Yang, K. Zhang, Study on two operating conditions of a full-scale oxidation ditch for optimization of energy consumption and effluent quality by using CFD model, Water Res., 45 (2011) 3439–3452.
[12] H. Xie, J. Yang, Y. Hu, H. Zhang, Y. Yang, K. Zhang, X. Zhu, Y. Li, C. Yang, Simulation of flow field and sludge settling in a full-scale oxidation ditch by using a two-phase flow CFD model, Chem. Eng. Sci., 109 (2014) 296–305.
[13] Y. Liu, H. Shi, L. Xia, H. Shi, T. Shen, Z. Wang, G. Wang, Y. Wang, Study of operational conditions of simultaneous nitrification and denitrification in a Carrousel oxidation ditch for domestic wastewater treatment, Bioresour. Technol., 101 (2010) 901–906.
[14] W.-l. Wei, H.-c. Dai, Turbulence Model Theory and Engineering Applications, Shanxi Science Technology Press, Xi'an, 2006.
[15] A.M. Karpinska Portela, New Design Tools for Activated Sludge Process, Ph.D. Thesis, FEUP, University of Porto, Porto, Portugal, 2013.
[16] A.M. Karpinska, J. Bridgeman, CFD-aided modelling of activated sludge systems – a critical review, Water Res., 88 (2016) 861–879.
[17] S.A. Orszag, I. Staroselsky, W.S. Flannery, Y. Zhang, Chapter 4: Introduction to Renormalization Group Modeling of Turbulence, T.B. Gatski, M.Y. Hussaini, J.L. Lumley, Simulation and Modeling of Turbulent Flows, Oxford University Press Inc., New York, NY, 1996.
[18] T.-H. Shih, W.W. Liou, A. Shabbir, Z. Yang, J. Zhu, A new k-ε eddy viscosity model for high Reynolds number turbulent flows, Comput. Fluids, 24 (1995) 227–238.
[19] B.E. Launder, D.B. Spalding, The numerical computation of turbulent flows, Comput. Methods Appl. Mech. Eng., 3 (1974) 269–289.
[20] W. Rodi, Turbulence Models and Their Application in Hydraulics, IAHR Monograph, CRC Press, Delft, The Netherlands, 1993.
[21] S. Vedantam, J.B. Joshi, S.B. Koganti, Three-dimensional CFD simulation of stratified two-fluid Taylor-Couette flow, Can. J. Chem. Eng., 84 (2006) 279–288.
[22] H.C. Lien, T.Y. Hsieh, J.C. Yang, Bend-flow simulation using 2D depth-averaged model, J. Hydraul. Eng., 25 (1999) 1097–1108.
[23] W. Wei, Y. Liu, B. Lv, Numerical simulation of optimal submergence depth of impellers in an oxidation ditch, Desal. Water Treat., 57 (2016) 8228–8235.
[24] E.J. Finnemore, B.J. Franzini, Fluid Mechanics with Engineering Applications, 10th ed., McGraw-Hill Companies, Inc., New York, NY, 2002.